

DYNAMICAL GENERATION OF $J^P = \frac{3}{2}^-$ RESONANCES AND THE $\Lambda(1520)$ RESONANCE

SOURAV SARKAR, L. ROCA, E. OSET, V. K. MAGAS AND
M. J. VICENTE VACAS

*Departamento de Física Teórica and IFIC, Centro Mixto Universidad de
Valencia-CSIC,
Investigación de Paterna, Aptdo. 22085, 46071 Valencia, Spain*

The lowest order chiral Lagrangian is used to study s -wave interactions of the baryon decuplet with the octet of pseudoscalar mesons. The coupled channel Bethe Salpeter equation is used to obtain dynamically generated $\frac{3}{2}^-$ resonances in the partial wave amplitudes which provide a reasonable description to a number of 3 and 4-star resonances like $\Delta(1700)$, $\Lambda(1520)$, $\Sigma(1670)$, $\Sigma(1940)$, $\Xi(1820)$, $\Omega(2250)$ etc. The phenomenological introduction of d -wave channels in the coupled channel scheme along with the existing s -wave channels is shown to provide a much improved description of the $\Lambda(1520)$ resonance. The prediction of the absolute strength of the cross section in the reactions $K^-p \rightarrow \Lambda\pi^0\pi^0$ and $K^-p \rightarrow \Lambda\pi^+\pi^-$ provided by this scheme shows a good agreement with existing data.

1. Introduction

The introduction of unitary techniques in a chiral dynamical treatment of the meson baryon interaction has been very successful. It has led to good reproduction of meson baryon data with a minimum amount of free parameters, and has led to the dynamical generation of many low lying resonances which qualify as quasibound meson baryon states ^{1,2}. In particular, the application of these techniques to the s -wave scattering of the baryon octet and the pseudoscalar meson octet have led to the successful description of many $J^P = \frac{1}{2}^-$ resonances like the $N^*(1535)$, the $\Lambda(1405)$, the $\Lambda(1670)$ and the $\Sigma(1620)$ ^{3,4,5,6}. Naively one may expect that this scheme is not suitable for studying d -wave resonances due to a large number of unknown parameters in the corresponding chiral Lagrangian. However d -wave resonances could be studied in s -wave interactions of the meson octet with the baryon decuplet ^{7,8,9}, in which case chiral dynamics is quite predictive. Applying unitary techniques to the lowest order chiral Lagrangian we have been successful in generating a number of $\frac{3}{2}^-$ resonances. From the

information of the pole positions and couplings to the channels involved we could associate many of these resonances to the $N^*(1520)$, $\Delta(1700)$, $\Lambda(1520)$, $\Sigma(1670)$, $\Sigma(1940)$, $\Xi(1820)$ resonances tabulated by the Particle Data Group (PDG).

We then consider the dynamics of one of the above resonances, namely the $\Lambda(1520)$, which is capturing renewed attention, particularly since it appears invariably in searches of pentaquarks in photonuclear reactions like $\gamma p \rightarrow K^+ K^- p$ and $\gamma d \rightarrow K^+ K^- np$. In the simple picture ⁸ mentioned above, this resonance couples to the $\pi\Sigma^*(1385)$ and $K\Xi^*(1530)$ channels, particularly to the former one. With the $\pi^+\Sigma^{*-}$, $\pi^-\Sigma^{*+}$, $\pi^0\Sigma^{*0}$ masses 7 MeV above, 2 MeV above and 1 MeV below the nominal $\Lambda(1520)$ mass and the strong coupling of the resonance to $\pi\Sigma^*$, this state could qualify as a loosely bound $\pi\Sigma^*$ state. However, the lack of other relevant channels which couple to the quantum numbers of the resonance makes the treatment of ⁸ only semiquantitative. In particular, the $\Lambda(1520)$ appears at higher energy than the nominal one and with a large width of about 130 MeV, nearly ten times larger than the physical width. This large width is a necessary consequence of the large coupling to the $\pi\Sigma^*$ channel and the fact that the pole appears at energies above the $\pi\Sigma^*$ threshold. On the other hand, if we modify the subtraction constants of the meson baryon loop function to bring the pole below the $\pi\Sigma^*$ threshold, then the pole appears without imaginary part. Since the width of the $\Lambda(1520)$ resonance comes basically from the decay into the $\bar{K}N$ and $\pi\Sigma(1193)$, the introduction of these channels is mandatory to reproduce the shape of the $\Lambda(1520)$ resonance.

In ^{10,11} we phenomenologically include the $\bar{K}N$ and $\pi\Sigma$ channels into the set of coupled channels which build up the $\Lambda(1520)$. The novelty with respect to the other channels already accounted for ⁸, which couple in s -wave, is that the new channels couple in d -waves. The transition matrix elements for the d -wave channels $\bar{K}N$ and $\pi\Sigma$ to the s -wave channel $\pi\Sigma^*$ were parametrized in terms of unknown constants which were fitted to experimental values for the real and imaginary parts of the partial wave amplitudes for the reactions $\bar{K}N \rightarrow \bar{K}N$ and $\bar{K}N \rightarrow \pi\Sigma$. The coupling of the $\Lambda(1520)$ to the $\pi\Sigma^*$ channel is then a prediction of this scheme and we use this to study the reaction $K^- p \rightarrow \pi^0 \pi^0 \Lambda$ and $K^- p \rightarrow \pi^+ \pi^- \Lambda$ which are closely related to the strength of this coupling. The prediction of the absolute strength of the cross sections in the above two reactions close to and above the $\Lambda(1520)$ energy find a good agreement with data.

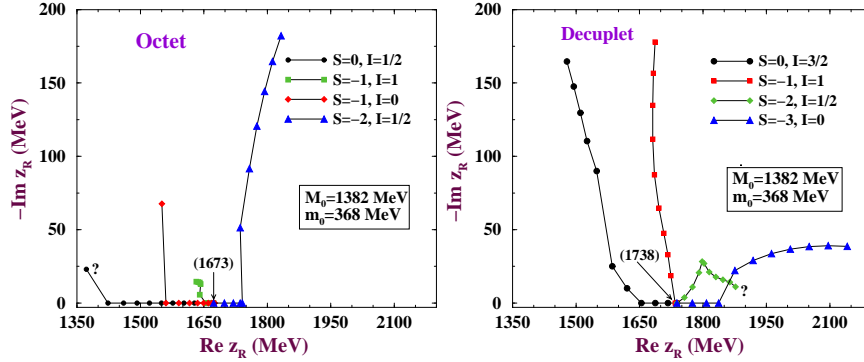


Figure 1. Trajectories of the poles in the scattering amplitudes obtained by increasing the value of the $SU(3)$ breaking parameter in steps of 0.1 (symbols) from zero, which is the $SU(3)$ symmetric situation, up to 1 which corresponds to the physical masses.

2. Dynamical generation of spin 3/2 baryon resonances

The tree-level scattering amplitude involving the baryon decuplet and the pseudoscalar octet is obtained from the dominant lowest order chiral Lagrangian which accounts for the Weinberg Tomozawa term. The matrix containing these amplitudes, V is used as the kernel of a coupled channel Bethe Salpeter equation given by

$$T = V + VGT \quad (1)$$

to obtain the transition matrix fulfilling exact unitarity in coupled channels. The factor G in the above equation is the meson baryon loop function. We have looked in detail^{8,9} at the $\frac{3}{2}^-$ resonances which are generated dynamically by this interaction, by searching for poles of the transition matrix in the complex plane in different Riemann sheets. We start from a $SU(3)$ symmetric situation where the masses of the baryons are made equal and the same is done with the masses of the mesons. In this case we found attraction in the octet, decuplet and the 27 representations, while the interaction was repulsive in the 35 representation. In the $SU(3)$ symmetric case all states of the $SU(3)$ multiplet are degenerate and the resonances appear as bound states with no width. As we gradually break $SU(3)$ symmetry by changing the masses, the degeneracy is broken and the states with different strangeness and isospin split apart generating pole trajectories in the complex plane which lead us to the physical situation in the final point, as seen in fig. 1. This systematic search allows us to trace the poles to their $SU(3)$ symmetric origin, although there is a mixing of representations

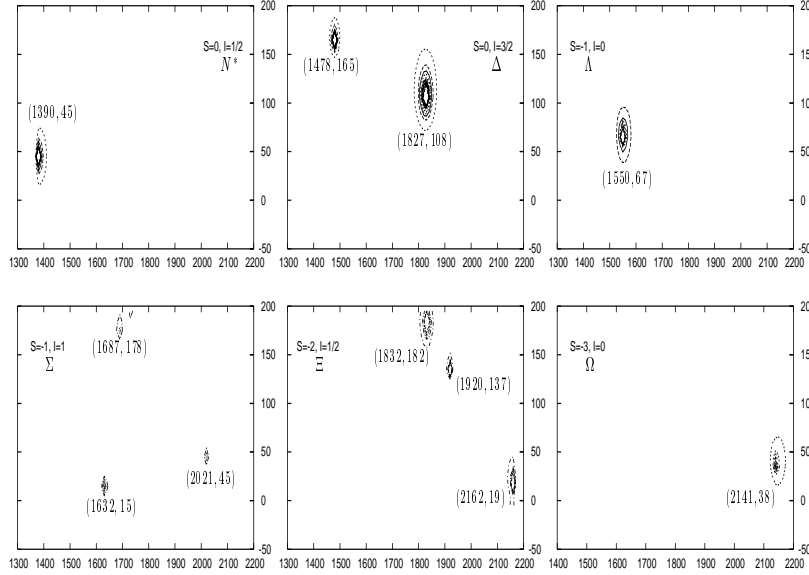


Figure 2. Contour plots of the scattering amplitudes showing poles in the unphysical Riemann sheets. The x and y axes denote the real and imaginary parts of the CM energy.

when the symmetry is broken.

In fig. 2 we show contour plots of the partial wave amplitudes as a function of the complex CM energy. The projection on the real (energy) axis is shown in fig. 3. We have also evaluated the residues of the poles from where the couplings of the resonances to the different coupled channels were found and this allowed us to make predictions for partial decay widths into a decuplet baryon and a meson. There is very limited experimental information on these decay channels but, even then, it represents an extra check of consistency of the results which allowed us to more easily identify the resonances found with some resonances known, or state that the resonance should correspond to a new resonance not yet reported by the PDG. In particular, in view of the information of the pole positions and couplings to channels we could associate some of the resonances found to the $N^*(1520)$, $\Delta(1700)$, $\Lambda(1520)$, $\Sigma(1670)$, $\Sigma(1940)$ and $\Xi(1820)$.

3. Improved description of the $\Lambda(1520)$ resonance

In addition to the transition amplitudes involving the s -wave channels $\pi\Sigma^*$ and $K\Xi^*$ which were used to dynamically generate the $\Lambda(1520)$ as discussed in the previous section we introduce phenomenologically tree level transition

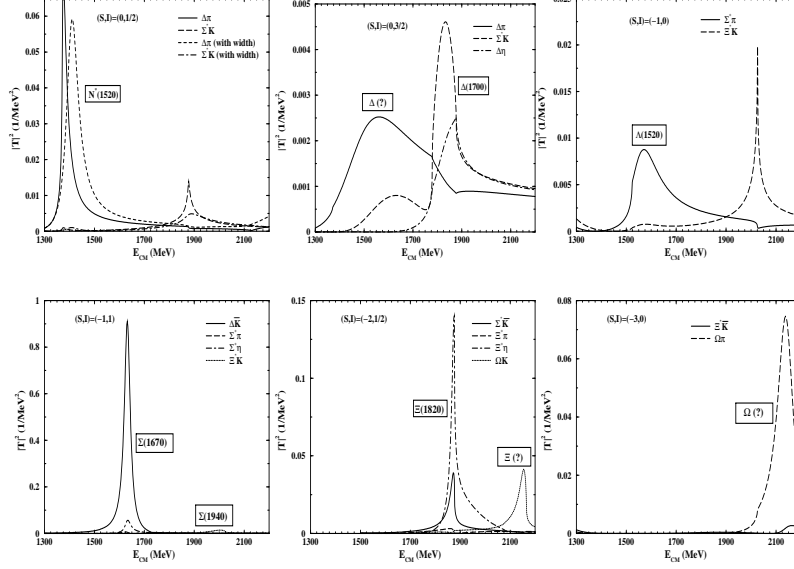


Figure 3. Scattering amplitudes as a function of CM energy showing $3/2^-$ resonances generated dynamically in decuplet baryon - pseudoscalar octet interactions.

potentials involving the d -wave channels $\bar{K}N$ and $\pi\Sigma$. As discussed in ¹⁰, we use for the vertices $\bar{K}N \rightarrow \bar{K}N$, $\bar{K}N \rightarrow \pi\Sigma$ and $\pi\Sigma \rightarrow \pi\Sigma$ effective transition potentials which are proportional to the incoming and outgoing momentum squared. Denoting $\pi\Sigma^*$, $K\Xi^*$, $\bar{K}N$ and $\pi\Sigma$ channels by 1, 2, 3 and 4 respectively, the matrix containing the tree level amplitudes is written as:

$$V = \begin{pmatrix} C_{11}(k_1^0 + k_1^0) & C_{12}(k_1^0 + k_2^0) & \gamma_{13} q_3^2 & \gamma_{14} q_4^2 \\ C_{21}(k_2^0 + k_1^0) & C_{22}(k_2^0 + k_2^0) & 0 & 0 \\ \gamma_{13} q_3^2 & 0 & \gamma_{33} q_3^4 & \gamma_{34} q_3^2 q_4^2 \\ \gamma_{14} q_4^2 & 0 & \gamma_{34} q_3^2 q_4^2 & \gamma_{44} q_4^4 \end{pmatrix}, \quad (2)$$

where $q_i = \frac{1}{2\sqrt{s}} \sqrt{[s - (M_i + m_i)^2][s - (M_i - m_i)^2]}$, $k_i^0 = \frac{s - M_i^2 + m_i^2}{2\sqrt{s}}$ and $M_i(m_i)$ is the baryon(meson) mass. The coefficients C_{ij} are $C_{11} = \frac{-1}{f^2}$, $C_{21} = C_{12} = \frac{\sqrt{6}}{4f^2}$ and $C_{22} = \frac{-3}{4f^2}$, where f is $1.15f_\pi$, with f_π ($= 93$ MeV) the pion decay constant, which is taken as an average between f_π and f_K . The elements V_{11} , V_{12} , V_{21} , V_{22} come from the lowest order chiral Lagrangian involving the decuplet of baryons and the octet of pseudoscalar mesons ^{8,7}. We neglect the elements V_{23} and V_{24} which involve the tree level interaction

of the $K\Xi^*$ channel to the d -wave channels because the $K\Xi^*$ threshold is far away from the $\Lambda(1520)$ and its role in the resonance structure is far smaller than that of the $\pi\Sigma^*$. It is also important to emphasize that the consideration of the width of the Σ^* resonance in the loop function G is crucial in order to account properly for the $\pi\Sigma^*$ channel since the threshold lies in the $\Lambda(1520)$ region. This is achieved through the convolution of the $\pi\Sigma^*$ loop function with the spectral distribution considering the Σ^* width.

In the model described so far we have as unknown parameters γ_{13} , γ_{14} , γ_{33} , γ_{34} , γ_{44} in the V matrix. Apart from these, there is also the freedom in the value of the subtraction constants in the loop functions. We will consider one subtraction constant for the s -wave channels (a_0) and one for the d -wave ones (a_2). Despite the apparent large number of free parameters in the V matrix, it is worth emphasizing that the largest matrix elements are V_{11} , V_{12} and V_{22} ⁸ which come from a chiral Lagrangian without any free parameters. Due to the d -wave behavior the other ones are expected to be smaller, as we will see below. In order to obtain these parameters we fit the partial wave amplitudes obtained by using the V matrix given above as the kernel in the Bethe-Salpeter equation to the experimental results on the $\bar{K}N$ and $\pi\Sigma$ scattering amplitudes in d -wave and $I = 0$. We use experimental data from^{12,13} where $\bar{K}N \rightarrow \bar{K}N$ and $\bar{K}N \rightarrow \pi\Sigma$ amplitudes are provided from partial wave analysis. These experimental amplitudes are related to the amplitudes of Eq. (1) through $\tilde{T}_{ij}(\sqrt{s}) = -\sqrt{\frac{M_i q_i}{4\pi\sqrt{s}}}\sqrt{\frac{M_j q_j}{4\pi\sqrt{s}}}T_{ij}(\sqrt{s})$, where M and q are the baryon mass and the on-shell C.M. momentum of the channel respectively. Note that in this normalization the branching ratio is simply given by the strength of the imaginary part as $B_i = \Gamma_i/\Gamma = \text{Im}\tilde{T}_{ii}(\sqrt{s} = M_R)$.

From the fit we obtain the subtraction constants $a_0 = -1.8$ for the s -wave channels and $a_2 = -8.1$ for the d -wave channels. The unknown constants in the V matrix are given by $\gamma_{13} = 0.98$ and $\gamma_{14} = 1.1$ in units of 10^{-7} MeV⁻³ and $\gamma_{33} = -1.7$, $\gamma_{44} = -0.7$ and $\gamma_{34} = -1.1$ in units of 10^{-12} MeV⁻⁵. We can see that the value obtained for the subtraction constant for the s -wave channels is of natural size (~ -2) since it agrees with the result obtained with the cutoff method using a cutoff of about 500 MeV (at $\sqrt{s} \simeq 1520$ MeV). On the other hand, regarding the d -wave loops, the large value obtained for a_2 can be understood comparing also to the cutoff method. If one keeps the momentum dependence of the d -wave vertices inside the loop integral (i.e., one does not use the on-shell approximation mentioned above) and evaluates the integral with the cutoff

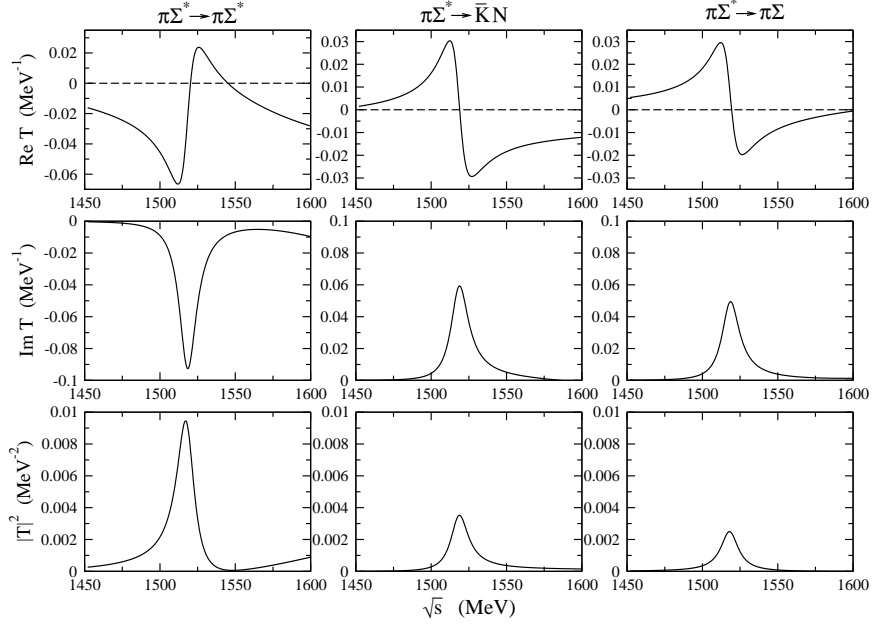


Figure 4. Unitary amplitudes involving the $\pi\Sigma^*$ channel. From left to right: $\pi\Sigma^* \rightarrow \pi\Sigma^*$, $\pi\Sigma^* \rightarrow \bar{K}N$ and $\pi\Sigma^* \rightarrow \pi\Sigma$.

method, then also a cutoff of about 500 MeV gives the same result as the dimensional regularization with on-shell factorization and $a_2 \sim -8$. In summary, the use of the dimensional regularization method along with the on-shell factorization for both the s and d -wave loops, correspond to the result obtained with the cutoff method without on-shell factorization using the same cutoff of about 500 MeV.

We now show in fig. 4, the prediction for the unitarized amplitudes for the different channels involving the $\pi\Sigma^*$. From left to right the columns represent the $\pi\Sigma^* \rightarrow \pi\Sigma^*$, $\pi\Sigma^* \rightarrow \bar{K}N$ and $\pi\Sigma^* \rightarrow \pi\Sigma$ channels. The rows denote from top to bottom the real part, imaginary part and modulus squared of the amplitudes (T_{ij}) respectively. We do not show the $K\Xi^*$ channel since it is less relevant as an external state in physical processes.

From the imaginary part of the amplitudes it is straightforward to obtain the couplings of the $\Lambda(1520)$ to the different channels in the following way. Close to the peak the amplitudes can be approximated by

$$T_{ij}(\sqrt{s}) = \frac{g_i g_j}{\sqrt{s} - M_{\Lambda(1520)} + i\Gamma_{\Lambda(1520)}/2} \quad (3)$$

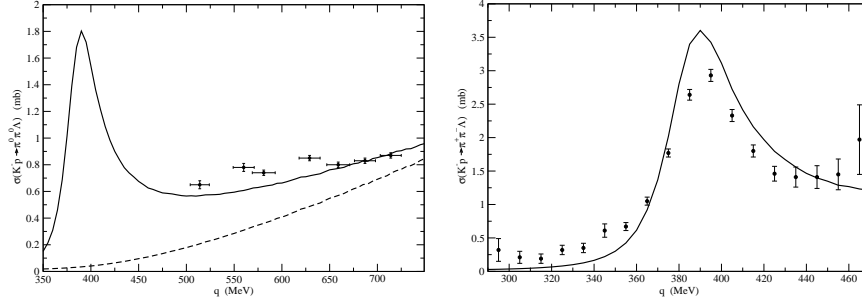


Figure 5. Result for the $K^-p \rightarrow \pi^0 \pi^0 \Lambda$ (left) and $K^-p \rightarrow \pi^+ \pi^- \Lambda$ (right) cross section.

from where we have

$$g_i g_j = -\frac{\Gamma_{\Lambda(1520)}}{2} \frac{|T_{ij}(M_{\Lambda(1520)})|^2}{\text{Im}[T_{ij}(M_{\Lambda(1520)})]}, \quad (4)$$

where $M_{\Lambda(1520)}$ is the position of the peak in $|T_{ij}|^2$ and $\Gamma_{\Lambda(1520)} = 15.6$ MeV. Up to a global sign of one of the couplings (we choose g_1 to be positive), we obtain: $g_1 = 0.91$, $g_2 = -0.29$, $g_3 = -0.54$ and $g_4 = -0.45$ for the coupling of the $\Lambda(1520)$ to the $\pi\Sigma^*$, $K\Sigma^*$, $\bar{K}N$ and $\pi\Sigma$ channels respectively. We can see from the values that the $\Lambda(1520)$ resonance couples most strongly to the $\pi\Sigma^*$ channel. The fact that we are able to predict the value of this coupling is a non trivial consequence of the unitarization procedure that we employ. With the value for g_1 obtained above, we can evaluate the partial decay width of the $\Lambda(1520)$ into $\pi\pi\Lambda$ assuming that this process is dominated by the $\pi\Sigma^*$ channel, and this leads us to a branching ratio of 0.14. All these branching ratios (the branching ratios obtained for $\bar{K}N$ and $\pi\Sigma$ are 0.45 and 0.43 respectively) essentially sum up to unity considering the uncertainties in the calculations.

The prediction of the amplitudes involving $\pi\Sigma^*$ channels can be checked in particular reactions where this channel could play an important role. We evaluate the cross section for $K^-p \rightarrow \pi\pi\Lambda$ in the lines of ¹⁰ but using the new coupled channel formalism. The mechanisms and the expressions for the amplitudes and the cross sections can be found in ¹⁰ where, apart from the coupled channel unitarized amplitude, other mechanisms of relevance above the $\Lambda(1520)$ peak were also included. In fig. 5 we show our results for $K^-p \rightarrow \pi^0 \pi^0 \Lambda$ and $K^-p \rightarrow \pi^+ \pi^- \Lambda$ cross section on the left and right panels respectively along with experimental data from refs. ¹⁵ and ¹⁶ respectively. The dashed line in the left figure represents the contribution from mechanisms other than the unitarized coupled channels, and the solid

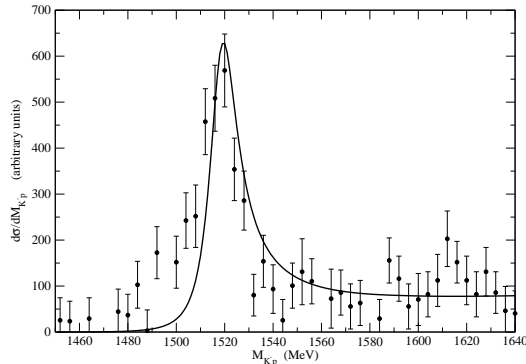


Figure 6. K^-p invariant mass distribution for the $\gamma p \rightarrow K^+ K^- p$ reaction with photons in the range $E_\gamma = 2.8 - 4.8$ GeV. Experimental data from ¹⁷.

line gives the coherent sum of all the processes. These cross sections depend essentially on the $T_{\bar{K}N \rightarrow \pi \Sigma^*}$ amplitude which is obtained from our coupled channel analysis. It is a non-trivial prediction of the theory since this amplitude has not been included in the fit.

We have also evaluated the K^-p invariant mass distribution for the $\gamma p \rightarrow K^+ K^- p$ reaction. In ¹⁴ the basic phenomenological model is explained but there only the $\pi \Sigma^*$ and $K \Xi^*$ channels were considered. The result in the present model is shown in Fig. 6. The normalization is arbitrary in the experimental data as well as in our calculation. For the purpose of the present work the shape of the distribution is the most important part and we can see that the agreement is quite fair.

4. Conclusions

We have done a coupled channel analysis of the $\Lambda(1520)$ resonance using the $\pi \Sigma^*$, $K \Xi^*$, $\bar{K} N$ and $\pi \Sigma$ channels. We have used the Bethe-Salpeter equation to implement unitarity in the evaluation of the different amplitudes. The main novelty from previous coupled channel approaches to this resonance is the inclusion of new matrix elements in the kernel of the Bethe-Salpeter equation and the consideration of the Σ^* width in the $\pi \Sigma^*$ loop function. The unknown parameters in the V matrix, as well as the subtraction constants of the loop functions, have been obtained by a fit to $\bar{K} N \rightarrow \bar{K} N$ and $\bar{K} N \rightarrow \pi \Sigma$ partial wave amplitudes. As a consequence of the unitarity of the scheme used, we can predict the amplitudes and couplings of the $\Lambda(1520)$ for all the different channels. The largest coupling is

obtained for the $\pi\Sigma^*$ channel.

We have then tested the amplitudes obtained in several specific reactions and compared with experimental data at energies close to and slightly above the $\Lambda(1520)$ region. These include the $K^-p \rightarrow \Lambda\pi^0\pi^0$, $K^-p \rightarrow \Lambda\pi^+\pi^-$ and $\gamma p \rightarrow K^+K^-p$ reactions. We have obtained a reasonable agreement with the experimental results that allows us to be confident in the procedure followed to describe the nature of the $\Lambda(1520)$ resonance.

Acknowledgments

This work is partly supported by DGICYT contract number BFM2003-00856, and the E.U. EURIDICE network contract no. HPRN-CT-2002-00311. This research is part of the EU Integrated Infrastructure Initiative Hadron Physics Project under contract number RII3-CT-2004-506078.

References

1. N. Kaiser, P. B. Siegel and W. Weise, Nucl. Phys. A **594** (1995) 325; N. Kaiser, T. Waas and W. Weise, Nucl. Phys. A **612** (1997) 297.
2. E. Oset and A. Ramos, Nucl. Phys. A **635** (1998) 99.
3. T. Inoue, E. Oset and M. J. Vicente Vacas, Phys. Rev. C **65** (2002) 035204.
4. D. Jido, J. A. Oller, E. Oset, A. Ramos and U. G. Meissner, Nucl. Phys. A **725** (2003) 181.
5. E. Oset, A. Ramos and C. Bennhold, Phys. Lett. B **527** (2002) 99 [Erratum-ibid. B **530** (2002) 260]; A. Ramos, E. Oset and C. Bennhold, Phys. Rev. Lett. **89** (2002) 252001.
6. C. Garcia-Recio, J. Nieves, E. Ruiz Arriola and M. J. Vicente Vacas, Phys. Rev. D **67** (2003) 076009.
7. E. E. Kolomeitsev and M. F. M. Lutz, Phys. Lett. B **585** (2004) 243; M. F. M. Lutz and E. E. Kolomeitsev, Nucl. Phys. A **755** (2005) 29.
8. S. Sarkar, E. Oset and M. J. Vicente Vacas, Nucl. Phys. A **750** (2005) 294; Eur. Phys. J. A **24** (2005) 287.
9. M. J. Vicente Vacas, E. Oset and S. Sarkar, Int. J. Mod. Phys. A **20** (2005) 1826; S. Sarkar, E. Oset and M. J. Vicente Vacas, Nucl. Phys. A **755** (2005) 665; E. Oset, S. Sarkar, M. J. Vicente Vacas, A. Ramos, D. Jido, J. A. Oller and U. G. Meissner, Int. J. Mod. Phys. A **20** (2005) 1619.
10. S. Sarkar, E. Oset and M. J. Vicente Vacas, Phys. Rev. C **72** (2005) 015206.
11. L. Roca, S. Sarkar, V. K. Magas and E. Oset, (in preparation).
12. G. P. Gopal *et al.*, Nucl. Phys. B **119** (1977) 362.
13. M. Alston-Garnjost *et al.*, Phys. Rev. D **18** (1978) 182.
14. L. Roca, E. Oset and H. Toki, arXiv:hep-ph/0411155.
15. S. Prakhov *et al.*, Phys. Rev. C **69** (2004) 042202.
16. T. S. Mast *et al.*, Phys. Rev. D **7** (1973) 5.
17. D. P. Barber *et al.*, Z. Phys. C **7** (1980) 17.